Original Research

VPO1 Promotes Programmed Necrosis of Cardiomyocytes in Rats with Chronic Heart Failure by Upregulating CYLD

Yinzhuang Zhang[1], Zhijie Shen[1], Zhuoni Mao[1], Dan Huang[1], Chengyu Lou[1],
Li Fang[1,*]

[1]Department of Cardiovascular Medicine, The Affiliated Changsha Hospital of Xiangya School of Medicine, Central South University, 410008 Changsha, Hunan, China
*Correspondence: fl20083@sina.com (Li Fang)

Abstract

Background: Chronic heart failure (CHF) is a serious cardiovascular condition. Vascular peroxidase 1 (VPO1) is associated with various cardiovascular diseases, yet its role in CHF remains unclear. This research aims to explore the involvement of VPO1 in CHF. **Methods**: CHF was induced in rats using adriamycin, and the expression levels of VPO1 and cylindromatosis (CYLD) were assessed. In parallel, the effects of VPO1 on programmed necrosis in H9c2 cells were evaluated through cell viability assays, lactate dehydrogenase (LDH) level measurements, and analysis of receptor-interacting protein kinase 1/receptor-interacting protein kinase 3/mixed lineage kinase domain-like protein (RIPK1/RIPK3/MLKL) pathway-related proteins. The impact of CYLD on RIPK1 protein stability and ubiquitination was also investigated, along with the interaction between VPO1 and CYLD. Additionally, cardiac structure and function were assessed using echocardiography, Hematoxylin-eosin (HE) staining, Masson staining, and measurements of myocardial injury-related factors, including N-terminal prohormone of brain natriuretic peptide (NT-proBNP), Aspartate aminotransferase (AST), LDH, and creatine kinase-myocardial band (CK-MB). **Results**: VPO1 expression was upregulated in CHF rats and in H9c2 cells treated with adriamycin. In cellular experiments, VPO1 knockdown improved cell viability, inhibited necrosis and the expression of proteins associated with the RIPK1/RIPK3/MLKL pathway. Mechanistically, VPO1 promoted cardiomyocyte programmed necrosis by interacting with the deubiquitinating enzyme CYLD, which enhanced RIPK1 ubiquitination and degradation, leading to activation of the RIPK1/RIPK3/MLKL signaling pathway. At animal level, overexpression of CYLD counteracted the cardiac failure, cardiac hypertrophy, myocardial injury, myocardial fibrosis, and tissue necrosis caused by VPO1 knockdown. **Conclusions**: VPO1 exacerbates cardiomyocyte programmed necrosis in CHF rats by upregulating CYLD, which activates the RIPK1/RIPK3/MLKL signaling pathway. Thus, VPO1 may represent a potential therapeutic target for CHF.

Keywords: VPO1; chronic heart failure; programmed necrosis; CYLD; RIPK1/RIPK3/MLKL

1. Introduction

Chronic heart failure (CHF) represents a significant public health challenge globally, characterized by the heart's inability to efficiently pump blood to satisfy the body's needs [1]. Patients with CHF commonly experience symptoms such as fatigue, shortness of breath, and reduced physical activity, which can severely impact their quality of life [2]. Additionally, CHF may lead to complications such as lung infections and arrhythmias, and in severe cases, it can be life-threatening [3]. Current treatments for CHF primarily include diuretics, angiotensin-converting enzyme (ACE) inhibitors, β-blockers, and other related therapies [3–5]. Despite their benefits, these treatments have limitations: long-term use of diuretics can cause electrolyte imbalances and hypokalemia [4], ACE inhibitors may result in dry cough and low blood pressure [6], and β-blockers while reducing heart rate and cardiac workload, can lead to bradycardia in some patients [7]. Although pacemakers and defibrillators can improve heart rhythm and prevent sudden death, their use is sometimes constrained by surgical risks [8]. Given these limitations and potential adverse effects, there is a pressing need to explore more effective and safer treatment strategies to enhance the quality of life for CHF patients.

A critical pathological feature of CHF is the significant loss of myocardial cells [9], which is closely associated with programmed cell necrosis [10]. The receptor-interacting protein kinase 1/receptor-interacting protein kinase 3/mixed lineage kinase domain-like protein (RIPK1/RIPK3/MLKL) signaling pathway is essential for regulating programmed cell necrosis [11–13]. In this pathway, RIPK1 forms a complex with RIPK3, leading to the activation of inflammatory necrosis and endogenous necrosis pathways [11]. MLKL, a substrate of RIPK3, is phosphorylated by RIPK3 [12], causing MLKL to translocate to the cell membrane, where it disrupts membrane integrity and induces cell death [13]. Additionally, the RIPK1/RIPK3/MLKL signaling pathway interacts with cylindromatosis (CYLD) [14]. CYLD, a deubiquitinating enzyme, plays a crucial role in regulating cell apoptosis and

inflammation by removing ubiquitin from RIPK1, thus inhibiting RIPK1-mediated cell death [15,16]. Furthermore, CYLD can modulate the activation of RIPK3 and MLKL, influencing the necroptosis process [17].

Cell necrosis is often linked to inflammation [18, 19]. During inflammatory responses, Vascular peroxidase 1 (VPO1) regulates oxidative stress [20]. VPO1-mediated reactions facilitate ubiquitination and intracellular signaling processes [21]. VPO1 is implicated in the development of various cardiovascular diseases, including atherosclerosis, coronary heart disease, and hypertension [22,23]. However, the specific mechanisms and roles of VPO1 in CHF require further investigation.

Therefore, this study aims to elucidate the role of VPO1 in cardiomyocyte programmed necrosis in rats with CHF and to identify key regulatory factors involved in the pathological processes of CHF at the molecular level. Additionally, we investigated the roles of CYLD and the RIPK1/RIPK3/MLKL signaling pathway in this context to identify new therapeutic targets for the clinical management of CHF.

2. Materials and Methods

2.1 Animals

Male Sprague-Dawley rats, aged 8 weeks and weighing 220–250 g, were procured from Hunan SJA Laboratory Animal Co., Ltd. (Changsha, China). They were acclimated for one week prior to the initiation of experimental procedures. They were randomly assigned to one of 6 groups: Control, Model, Model + small interfering RNA-negative control (Model + si-NC), Model + small interfering RNA for VPO1 (Model + si-VPO1), Model + si-VPO1 + overexpressed negative control (Model + si-VPO1 + oe-NC), and Model + si-VPO1 + overexpressed CYLD vector (Model + si-VPO1 + oe-CYLD), with 5 rats per group. The Model group received weekly intraperitoneal injections of 2.0 mg/kg adriamycin (ADR, 25316-40-9, Shanghai Yuanye Bio-Technology Co., Ltd, Shanghai, China) for 6 consecutive weeks to construct the CHF rat model [24]. In addition to ADR, rats in the Model + si-NC, Model + si-VPO1, Model + si-VPO1 + oe-NC, and Model + si-VPO1 + oe-CYLD groups were also administered 500 µL of 8×10^5 TU of the respective lentiviral vectors: si-NC, si-VPO1, si-VPO1 + oe-NC, and si-VPO1 + oe-CYLD [25]. Throughout the experiment, the health of the animals was closely monitored, and no mortality was observed. For euthanasia, cervical dislocation was employed to ensure rapid death. All experimental procedures and animal handling were conducted in accordance with the approval of the Animal Care and Use Committee of the Affiliated Changsha Hospital of Xiangya School of Medicine, Central South University (No. 2021-69).

2.2 Cell Culture and Treatment

Rat myocardial cells, H9c2 (AW-CNR083, Abiowell, Changsha, China), were cultivated in Dulbecco's modified Eagle's medium (DMEM, AW-M003, Abiowell) supplemented with 10% fetal bovine serum (10099141, Gibco, Grand Island, NY, USA) and 1% penicillin/streptomycin solution (AWH0529a, Abiowell) and maintained in an incubator at 37 °C with 5% CO_2. All cell lines were validated by STR profiling and tested negative for Mycoplasma sp.

H9c2 cells were categorized into six groups: Control, Model, Model + si-NC, Model + si-VPO1, Model + si-VPO1 + oe-NC, and Model + si-VPO1 + oe-CYLD. Cells in the Model group were treated with 0.5 µmol/L ADR for 24 h [26]. Cells in the Model + si-NC group were transfected with si-NC for 20 min following ADR treatment. For the Model + si-VPO1 group, H9c2 cells were transfected with si-VPO1 (5′-GGGCAGAGATACAGCACATCA-3′) for 20 min post-ADR treatment. In the Model + si-VPO1 + oe-NC and Model + si-VPO1 + oe-CYLD groups, cells were transfected with oe-NC and oe-CYLD, respectively, in addition to the si-VPO1 treatment.

2.3 Reverse Transcription-Quantitative Polymerase Chain Reaction (RT-qPCR)

Total RNA was extracted from rat myocardial tissues and H9c2 cells using the Trizol reagent (15596026, Thermo Fisher Scientific, Waltham, MA, USA) following the manufacturer's instructions. After converting the RNA to cDNA with the effective mRNA reverse transcription kit (CW2569, Beijing CoWin Biotech, Beijing, China), 2 µL of cDNA was used for RT-qPCR analysis on a QuantStudio1 system (ABI, Carlsbad, CA, USA). The reaction conditions were as follows: initial denaturation at 95 °C for 10 min, followed by 40 cycles of amplification at 95 °C for 15 seconds and 60 °C for 30 seconds. The relative mRNA levels of target genes were calculated using the $2^{-\triangle\triangle Ct}$ method. Specific primer sequences are detailed in Table 1.

2.4 Western Blot (WB)

Total protein was extracted from rat myocardial tissues and H9c2 cells. The BCA protein quantification kit (AWB0156, Abiowell) was used to determine the protein concentration. Proteins were mixed with 5× loading buffer (AWB0055, Abiowell), boiled for 5 min, and then rapidly cooled on ice. Electrophoresis was performed at a constant voltage of 75 V for 130 min. The process was halted when the bromophenol blue dye reached the bottom of the gel. Proteins were then transferred to nitrocellulose membranes using electrophoresis at 300 mA. Next, the membranes were rinsed once with 1× phosphate-buffered saline with Tween 20 (1× PBST, AWI0130a, Abiowell) and blocked by immersion in 1× PBST containing 5% skimmed milk and shaken for 90 min. Primary antibodies were incubated with the membranes overnight at 4 °C. Secondary antibodies were applied for 1.5 h at room temperature. Details of the

Table 1. Specific primer sequences.

Gene	Primer sequence	Product length
R-*VPO1*	F: 5′-TGCCTCTCTAGAGCAACTGT-3′ R: 5′-CCAACTGACTGAACGTCCCA-3′	146 bp
R-*RIPK1*	F: 5′-CTTAGACGCGTAGGAGCGG-3′ R: 5′-GACGGAGCTAGGTGCTGAAG-3′	173 bp
R-*RIPK3*	F: 5′-GCAAGGAGTCAGGGGAATCA-3′ R: 5′-TGGGTTTGGAAGGATGCTCG-3′	244 bp
R-*MLKL*	F: 5′-GCGCAGGATAGACCAAGACC-3′ R: 5′-TTATCCATACCCCGAGTTCCAG-3′	140 bp
R-*GAPDH*	F: 5′-ACAGCAACAGGGTGGTGGAC-3′ R: 5′-TTTGAGGGTGCAGCGAACTT-3′	252 bp

VPO1, Vascular peroxidase 1; *RIPK1*, receptor-interacting protein kinase 1; *RIPK3*, receptor-interacting protein kinase 3; *MLKL*, mixed lineage kinase domain-like protein.

Table 2. Specific information about the antibodies.

Name	Catalog	Dilution ratio	Company
VPO1	ABS1675	1:1000	Merck KGaA, Darmstadt, Germany
p-RIPK1	AWA48187	1:1000	Abiowell, Changsha, China
RIPK1	AWA48186	1:2000	Abiowell, Changsha, China
p-RIPK3	AWA57678	1:2000	Abiowell, Changsha, China
RIPK3	AWA57677	1:1000	Abiowell, Changsha, China
p-MLKL	AWA10442	1:5000	Abiowell, Changsha, China
MLKL	AWA51934	1:2000	Abiowell, Changsha, China
CYLD	AWA55911	1:2000	Abiowell, Changsha, China
A20	AWA44305	1:1000	Abiowell, Changsha, China
Ovarian tumor deubiquitinase 1 (OTUD1)	29921-1-AP	1:2000	Proteintech, Chicago, IL, USA
Ovarian tumor deubiquitinase 7B (OTUD7B)	AWA50003	1:2000	Abiowell, Changsha, China
Ovarian tumor deubiquitinase with linear linkage specificity (OTULIN)	AWA53412	1:1000	Abiowell, Changsha, China
Glyceraldehyde 3-phosphate dehydrogenase (GAPDH)	AWA80009	1:5000	Abiowell, Changsha, China
HRP goat anti-rabbit IgG (H+L)	AWS0002	1:5000	Abiowell, Changsha, China

CYLD, cylindromatosis; A20, tumor necrosis factor α-induced protein 3; HRP, horseradish peroxidase.

antibodies used are provided in Table 2. After incubation, the membranes were washed three times with 1× PBST. Lastly, the enhanced chemiluminescence (ECL) solution (AWB0005, Abiowell) was applied to the membranes, and protein bands were visualized using a chemiluminescent imaging system (ChemiScope6100, Clinx Science Instruments, Shanghai, China).

2.5 Detection of Protein Stability

To assess protein stability, proteins were treated with 50 µg/mL cycloheximide (CHX, 583794, Gentihold, Beijing, China) for 0, 1, 2, and 3 h. The treated proteins were then analyzed according to the WB procedure described above [27].

2.6 Immunohistochemistry (IHC) Staining

The myocardial tissue sections were first baked, placed in xylene and subjected to ethanol at concentrations of 100%, 95%, 85%, and 75%. For antigen retrieval, the sections were immersed in 0.01 mol/L citrate buffer (AWT0732a, Abiowell), microwaved to boiling, and allowed to cool for 20 min. After rinsing three times with phosphate-buffered saline (PBS, AWR0213a, Abiowell), the antigen retrieval process was completed. Sections were treated with 1% periodate (AWI0186a, Abiowell) at room temperature for 10 min to block endogenous enzyme activity, followed by three rinses with PBS. Primary antibody VPO1 (PA5-144080, 1:200, Thermo Fisher Scientific) was incubated with the sections overnight at 4 °C. Secondary antibody horseradish peroxidase (HRP) goat anti-rabbit IgG (SA00001-2, 1:1000, Proteintech, Chicago, IL, USA) was applied to the sections for 30 min at 37 °C. The sections were then treated with the diaminobenzidine (DAB) working solution (ZLI9017, Zsbio, Beijing, China) for color development. Following re-staining with hematoxylin (AWI0009a, Abiowell) and dehydration through graded alcohol (60–100%) for 5 min each, the sections were cleared in xylene. Finally, the sections were mounted and examined under a microscope (DSZ2000X, Cnmicro, Beijing, China).

2.7 Cell Counting Kit-8 (CCK-8)

Cells in the logarithmic growth phase were harvested, counted, and seeded at a density of 5×10^3 cells/well into 96-well plates, with three replicate wells per group. Each well was filled with medium containing 10% CCK-8 (AWC0114a, Abiowell) and incubated at 37 °C with 5% CO_2. Absorbance at 450 nm was measured using an enzyme-labeled instrument (MB-530, Heleas, Shenzhen, China).

2.8 Reagent Kit Detection

The cellular lactate dehydrogenase (LDH) level was measured using the LDH assay kit (A020-2, Nanjing Jiancheng Bioengineering Institute, Nanjing, China) according to the manufacturer's instructions. The N-terminal prohormone of brain natriuretic peptide (NT-proBNP) level was assessed with the NT-proBNP kit (CSB-E08752r, Cusabio, Wuhan, China). Aspartate aminotransferase (AST) levels were determined using the AST assay kit (C010-2-1, Nanjing Jiancheng Bioengineering Institute, Nanjing, China). The creatine kinase-myocardial band (CK-MB) level in myocardial tissues was evaluated with the CK-MB kit (CSB-E14403r, Cusabio).

2.9 Flow Cytometry

The cells were stained with 30.0 µL of fluorochrome-labeled inhibitor of pan-caspase (FLICA) staining solution (ab219935, Abcam, Cambridge, UK) for 1 h in the dark. Following staining, cells were rinsed with washing buffer (ab219935, Abcam). The cells were then mixed with propidium iodide (PI, ab219935, Abcam) and washed with PBS. Flow cytometry was performed using a flow cytometer (A00-1-1102, Beckman, Pasadena, CA, USA) to analyze the results.

2.10 Immunofluorescence (IF)

Detection of protein levels: H9c2 cell sections were rinsed with PBS and fixed in 4% paraformaldehyde (AWI0056a, Abiowell). Cells were permeabilized with 0.3% Triton X-100 (AWT0107a, Abiowell) for 30 min at 37 °C, followed by blocking with 5% bovine serum albumin (BSA, AWT0206a, Abiowell) for 60 min at 37 °C. Primary antibody RIPK1 (17519-1-AP, 1:50, Proteintech) was incubated with cells overnight at 4 °C. Goat anti-rabbit IgG (H+L) secondary antibody (AWS0005c, 1:200, Abiowell) was applied for 1.5 h at 37 °C. Nuclei were stained with the DAPI working solution (AWC0291a, Abiowell). Sections were mounted with buffered glycerol (AWI0178a, Abiowell) and visualized using a fluorescence microscope (BA410T, Motic, Xiamen, China).

Wheat Germ Agglutinin (WGA) Staining: Rat myocardial tissue sections were treated with sodium borohydride solution (C189300050, Sinopharm Chemical Reagent Co., Ltd, Shanghai, China). Sections were subsequently blocked with 0.3% hydrogen peroxide (80070961, Sinopharm Chemical Reagent Co., Ltd) and 5% BSA. Primary antibody Evans blue dye (EBD, bs-1558R, 1:100, Bioss, Beijing, China) was incubated with the sections overnight at 4 °C. Goat anti-rabbit IgG (H+L) secondary antibody was applied for 30 min at 37 °C. Sections were then reacted with TYP-570 (AWI0693a, Abiowell) and stained with WGA staining solution (W21405, Thermo Fisher Scientific). Nuclei were stained with the DAPI working solution. Tissue sections were cleared with Sudan Black solution and examined under a fluorescence microscope.

Detection of Co-localization: The rats' heart tissues were embedded and baked at 60 °C for 12 h. Sections were deparaffinized, treated with Tris-EDTA buffer (pH 9.0, AWI0117a, Abiowell), microwaved to boiling, cooled to room temperature, and washed with PBS for 3 min to complete antigen retrieval. Sections were then treated with sodium borohydride solution for 30 min at room temperature, followed by 75% ethanol for 1 min, Sudan Black B (AWI0468a, Abiowell) for 15 min, and 10% normal serum 5% BSA for 60 min. Primary antibody VPO1 (1:200) was incubated with the sections overnight at 4 °C. Secondary antibodies HRP goat anti-rabbit IgG (1:1000) were applied for 30 min at 37 °C. After rinsing with PBS, sections were incubated with TSA-520 fluorescent dye (AWI0693a, Abiowell) at 37 °C away from light. Moreover, this process was repeated using Troponin T (1:100, ABS1675, Merck KGaA, Darmstadt, Germany), Vimentin (1:100, 10366-1-AP, Proteintech), or platelet/endothelial cell adhesion molecule-1 (CD31, 1:100, 11265-1-AP, Proteintech) as primary antibodies and TSA-570 (AWI0693a, Abiowell) as the fluorescent dye. Nuclei were stained with DAPI at 37 °C. Sections were mounted with buffered glycerol and observed under a fluorescence microscope for documentation.

2.11 Co-Immunoprecipitation (Co-IP)

The cells were rinsed with PBS and lysed using IP cell lysate (AWB0144, Abiowell). After centrifugation, the supernatant was incubated overnight with VPO1 or RIPK1 antibodies. To capture antigen-antibody complexes, 20 µL of protein A/G agarose was added to the lysate and incubated with the antibodies at 4 °C for 2 h with gentle shaking. Following Co-IP, the levels of VPO1 and CYLD, as well as the expression of RIPK1 and Ubiquitin (#3936, 1:1000, Boston, MA, USA), were assessed by WB.

2.12 Echocardiographic Evaluation

Cardiac performance indices were calculated using Vevo software (Vevo 1100, VisualSonics, Canada). During surgery, rats were anesthetized with 2.5% isopropyl ether (80111128, Sinopharm Chemical Reagent Co., Ltd). Parameters analyzed included left ventricular ejection fraction (LVEF), left ventricular fractional shortening (LVFS), left ventricular end-systolic diameter (LVESD), and left ventricular end-diastolic diameter (LVEDD).
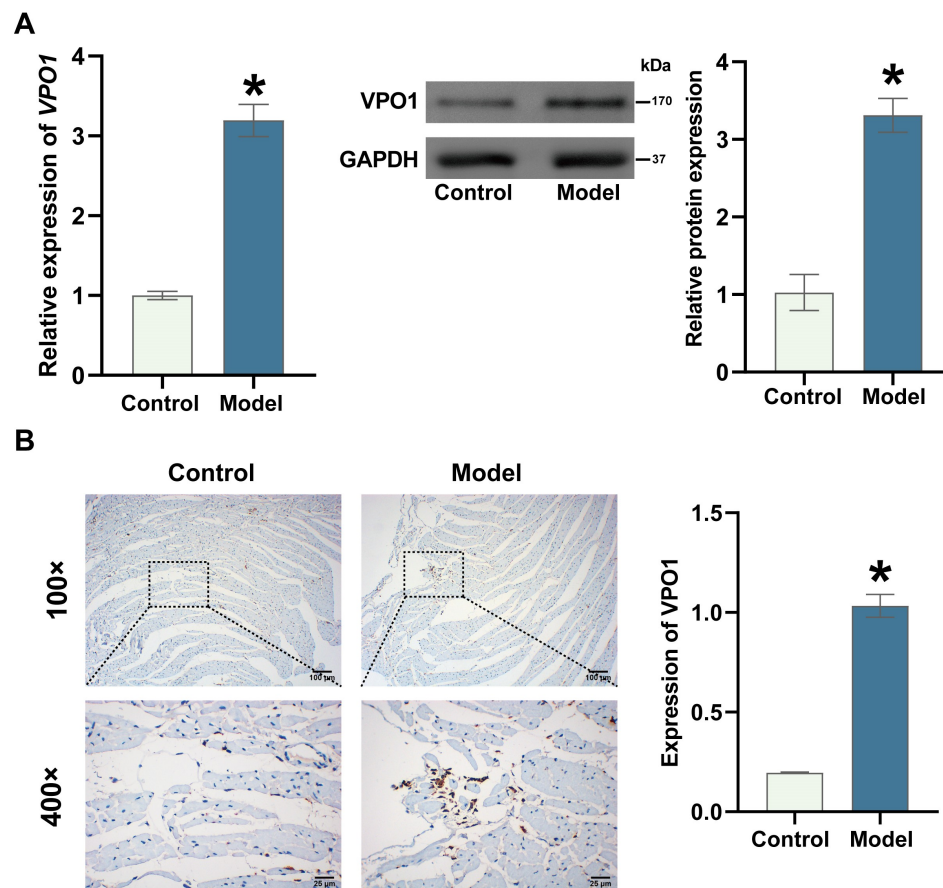
Fig. 1. Vascular peroxidase 1 (VPO1) was upregulated in rats with adriamycin (ADR)-induced Chronic heart failure (CHF). (A) Expression of VPO1 was assessed by reverse transcription-quantitative polymerase chain reaction (RT-qPCR) and western blot (WB). (B) VPO1 levels confirmed by Immunohistochemistry (IHC) staining. 400× scale bar = 25 µm, 100× scale bar = 100 µm. $^*p < 0.05$ vs. Control. n = 5.

2.13 Hematoxylin-Eosin (HE) Staining

Rat myocardial tissue sections were baked at 60 °C for 12 h. The sections were then immersed in xylene (10023418, Sinopharm) for 20 min, followed by sequential immersion in ethanol at concentrations of 100%, 100%, 95%, 85%, and 75% for 5 min each. Sections were stained with hematoxylin (AWI0009a, Abiowell) for 5 min, rinsed with distilled water and PBS, and then stained with eosin (AWI0032a, Abiowell) for 3 min. After dehydration with gradient alcohol (95–100%), sections were cleared in xylene for 10 min, mounted with neutral gum (G0503, Sigma, Saint Louis, MO, USA), and observed under a microscope.

2.14 Masson Staining

Myocardial fibrosis was assessed using a Masson staining kit (AWI0253a, Abiowell). Rat myocardial tissue sections were first baked. A sufficient amount of nuclear staining solution was applied dropwise to cover the entire section, and staining was performed for 1 min. The sections were then immersed in distilled water, followed by soaking in PBS for 5–10 min to restore the blue color of the cell nuclei. Next, the plasma staining solution was applied to the sections. After staining, the solution was discarded, and the sections were treated with a re-staining solution, and then rinsed with anhydrous ethanol. Finally, the tissue sections were dried, cleared with xylene, and sealed.

2.15 Statistical Analysis

Statistical analysis was performed using GraphPad Prism 8 software (8.0.2.263, San Diego, CA, USA). The data are presented as mean ± standard deviation (SD). Each experiment was performed in triplicate. Normal distribution was assessed, and comparisons between two groups were made using the T-test, while comparisons among multiple groups were conducted using One-way ANOVA. Statistical significance was set at $p < 0.05$.
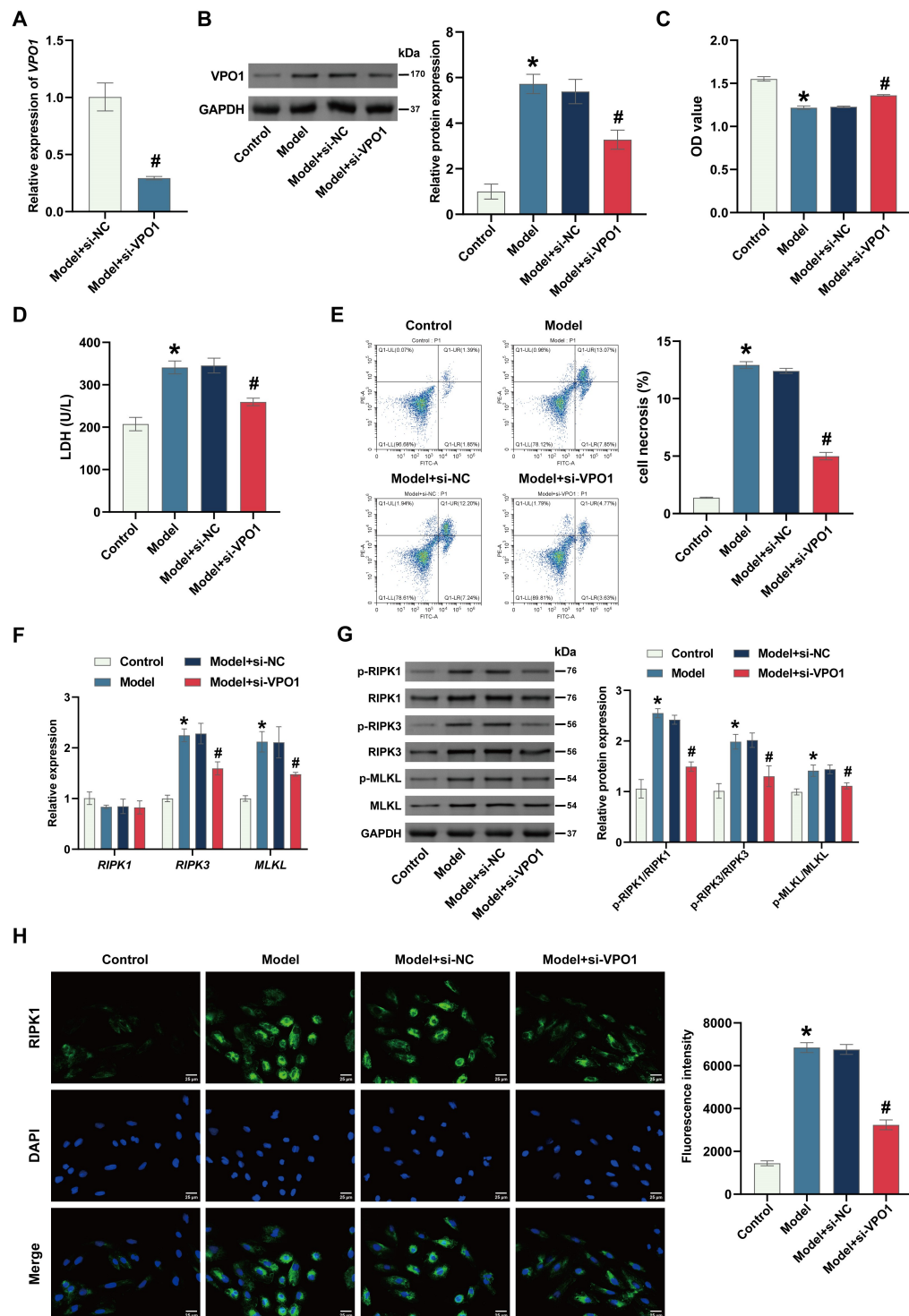
Fig. 2. VPO1 downregulation alleviates programmed necrosis in H9c2 cells. (A) *VPO1* mRNA levels were assessed by reverse transcription (RT)-qPCR. (B) VPO1 protein levels were evaluated by WB. (C) Optical density (OD) value. (D) LDH levels were measured with a kit. (E) Necrosis rate was detected by flow cytometry with Annexin V-FITC/PI staining. (F) mRNA levels of *RIPK1*, *RIPK3*, and *MLKL* were examined by RT-qPCR. (G) Phosphorylation of RIPK1, RIPK3, and MLKL was measured by WB. (H) RIPK1 protein levels were assessed by immunofluorescence (IF). Scale bar = 25 μm. $^*p < 0.05$ vs. Control. $^\#p < 0.05$ vs. Model + si-NC. n = 3. LDH, lactate dehydrogenase; *RIPK1*, receptor-interacting protein kinase 1; *RIPK3*, receptor-interacting protein kinase 3; *MLKL*, mixed lineage kinase domain-like protein; NC, negative control.
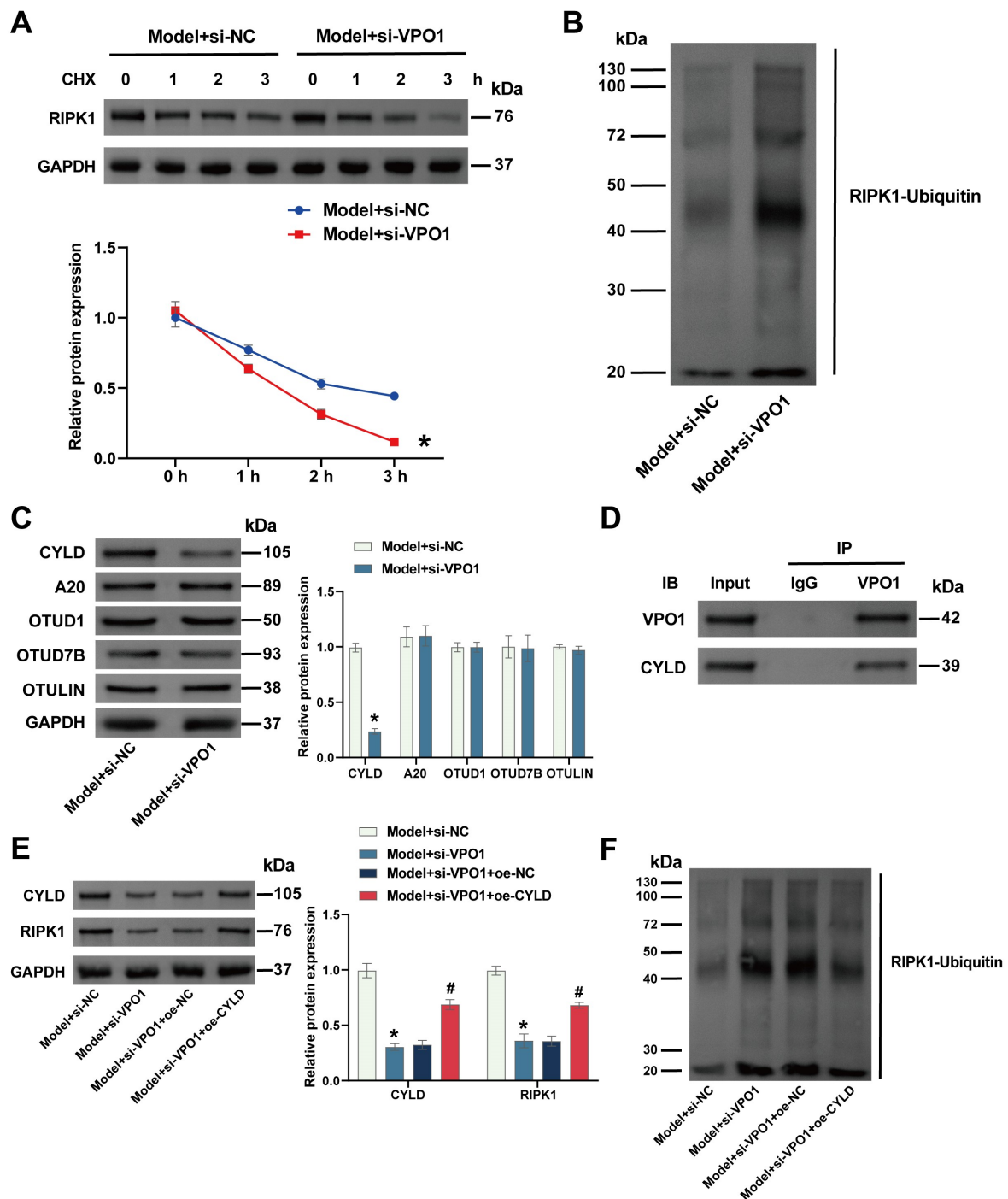
Fig. 3. VPO1 inhibits RIPK1 ubiquitination via deubiquitinase CYLD. (A) RIPK1 protein stability was assessed by WB. (B) RIPK1 ubiquitination was examined by Co-Immunoprecipitation (Co-IP). (C) Levels of deubiquitinases CYLD, A20, OTUD1, OTUD7b, and OTULIN were measured by WB. (D) Interaction between VPO1 and CYLD was visualized by Co-IP. (E) Levels of CYLD and RIPK1 were determined by WB. (F) RIPK1 ubiquitination was calculated by Co-IP. $^{*}p < 0.05$ vs. Model + si-NC. $^{\#}p < 0.05$ vs. Model + si-VPO1 + oe-NC. n = 3. oe, overexpressed.

3. Results

3.1 Upregulation of VPO1 in ADR-Induced CHF Rats

To investigate the role of VPO1 in CHF, we induced CHF in rat models using ADR. Our results demonstrated a significant upregulation of VPO1 expression in these CHF models (Fig. 1A). IHC further confirmed an elevated level of VPO1 in the Model group compared to controls (Fig. 1B). These findings suggested that VPO1 may play a role in CHF-related processes.
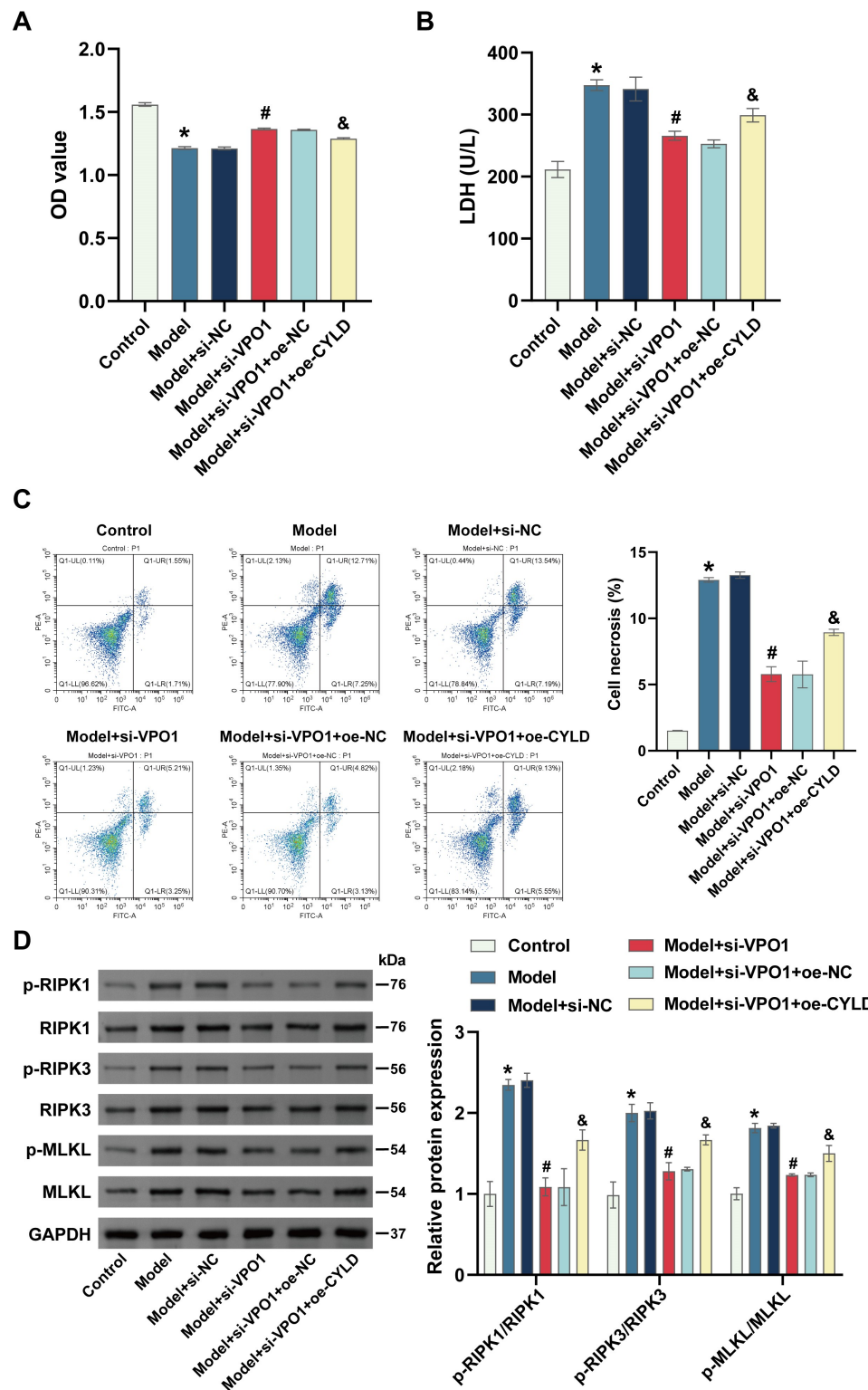
Fig. 4. VPO1 downregulation alleviates programmed necrosis in H9c2 cells via the CYLD/RIPK1 axis. (A) H9c2 cell viability was measured by Cell Counting Kit-8 (CCK-8) assay. (B) LDH levels were calculated using a kit. (C) Necrosis rate was detected by flow cytometry with Annexin V-fluorescein isothiocyanate/propidium iodide (Annexin V-FITC/PI) staining. (D) Phosphorylation levels of RIPK1, RIPK3, and MLKL were measured by WB. $^{*}p < 0.05$ vs. Control. $^{\#}p < 0.05$ vs. Model + si-NC. $^{\&}p < 0.05$ vs. Model + si-VPO1 + oe-NC. n = 3.

We also examined the expression of VPO1 in cardiomyocytes, fibroblasts, and endothelial cells derived from rat heart tissues. By using markers such as Troponin T for cardiomyocytes, vimentin for fibroblasts, and CD31 for endothelial cells [28], we performed co-localization studies. Our findings indicated that VPO1 co-localized with Troponin T, vimentin, and CD31. Moreover, CHF may affect VPO1 expression in cardiomyocytes, fibroblasts and endothelial cells, suggesting that VPO1 may also influence CHF pathology (**Supplementary Fig. 1A–C**).

3.2 Alleviation of Programmed Necrosis by VPO1 Downregulation in H9c2 Cells

To further explore the relationship between VPO1 and programmed necrosis in H9c2 cells, we transfected cells with *VPO1*-specific siRNA to silence VPO1 expression. Transfection with si-VPO1 markedly reduced *VPO1* levels (Fig. 2A). ADR administration upregulated VPO1 expression, whereas si-VPO1 transfection mitigated this increase (Fig. 2B). The level of LDH, a marker of cell necrosis [29], was also measured. Knockdown of *VPO1* reversed ADR-induced decreases in H9c2 cell viability and increases in LDH levels and cell necrosis (Fig. 2C–E). RIPK1, RIPK3, and MLKL are key markers of programmed cell necrosis [13]. Therefore, we assessed their relative expression and protein phosphorylation. At the mRNA level, VPO1 knockdown diminished RIPK3 and MLKL expression but had no effect on RIPK1 mRNA levels (Fig. 2F). At the protein level, VPO1 knockdown lowered the phosphorylation of RIPK1, RIPK3, and MLKL (Fig. 2G). Additionally, immunofluorescence analysis revealed a reduction in RIPK1 levels following *VPO1* knockdown (Fig. 2H). These findings suggest that VPO1 downregulation alleviates programmed necrosis in H9c2 cells.

3.3 VPO1 Inhibits RIPK1 Ubiquitination via Deubiquitinase CYLD

To explore the effect of VPO1 on RIPK1 ubiquitination, we employed cycloheximide (CHX) to inhibit protein synthesis, thereby promoting the gradual degradation of existing proteins and revealing their stability [27]. As exhibited in Fig. 3A, RIPK1 levels decreased progressively with increasing CHX treatment time. Notably, the knockdown of *VPO1* exacerbated the reduction in RIPK1 stability induced by CHX treatment (Fig. 3A). Additionally, *VPO1* knockdown led to increased ubiquitination of RIPK1 (Fig. 3B). Ubiquitination of RIPK1 is known to be regulated by deubiquitinases [30–34]. We measured the levels of several deubiquitinases, including CYLD [30], A20 [31], OTUD1 [32], OTUD7b [33], and OTULIN [34], using WB. However, *VPO1* knockdown specifically lowered CYLD levels without affecting other deubiquitinases (Fig. 3C). Furthermore, we observed that VPO1 interacted with CYLD (Fig. 3D), suggesting that VPO1 may inhibit RIPK1 ubiquitination through CYLD.

To further validate this, we overexpressed *CYLD*. Compared to the Model + si-VPO1 + oe-NC group, overexpression of CYLD increased both *CYLD* and RIPK1 levels while reducing RIPK1 ubiquitination (Fig. 3E,F). These results demonstrated that VPO1 inhibited RIPK1 ubiquitination via CYLD.

3.4 Alleviation of Programmed Necrosis by VPO1 Downregulation via the CYLD/RIPK1 Axis

Next, we investigated whether the alleviation of programmed necrosis in H9c2 cells by VPO1 downregulation was associated with the CYLD/RIPK1 axis. As depicted in Fig. 4A–C, overexpression of *CYLD* counteracted the reduction in H9c2 cell viability, lower LDH levels, and decreased cell necrosis observed with *VPO1* knockdown. Moreover, in contrast to the Model + si-VPO1 + oe-NC group, *CYLD* overexpression enhanced the phosphorylation of RIPK1, RIPK3, and MLKL (Fig. 4D). These findings suggested that VPO1 downregulation could alleviate programmed necrosis in H9c2 cells through the CYLD/RIPK1 axis.

3.5 VPO1 Downregulation Improves ADR-Induced CHF in Rats via the CYLD/RIPK1 Axis

Cellular programmed necrosis is tightly related to CHF [10]. To explore whether the downregulation of VPO1 could improve ADR-induced CHF in rats through the CYLD/RIPK1 axis, we utilized the CHF rat model for subsequent experiments. LVEF, LVFS, LVESD, and LVEDD are commonly recognized for evaluating cardiac structure and function [35]. As shown in Fig. 5A, rats in the Model group exhibited lowered LVEF and LVFS levels and elevated LVESD and LVEDD levels in contrast to the Control group, suggesting that CHF weakened heart function in rats. However, the knockdown of *VPO1* attenuated the decline in cardiac function of CHF mice, and this effect could be reversed by *CYLD* overexpression (Fig. 5B). Additionally, CHF is often accompanied by cardiac enlargement and thickening [36]. Thus, we determined the ratios of heart weight/body weight (HW/BW) and heart weight/tibia length (HW/TL). Compared to the Control group, the ratios of HW/BW and HW/TL were raised in the Model group, suggesting that the heart was enlarged and thickened under the impact of CHF. Comparatively, the knockdown of *VPO1* alleviated this phenomenon, but the role of *VPO1* knockdown was inhibited by overexpression of *CYLD* (Fig. 5B). Next, we observed the levels of myocardial damage and fibrosis in the left ventricle of rats. Rats in the Model group had exacerbated myocardial damage and myocardial fibrosis relative to the Control group. However, *VPO1* knockdown alleviated myocardial morphological damage and myocardial fibrosis and *CYLD* overexpression suppressed this ameliorative effect of *VPO1* knockdown on myocardial damage and fibrosis (Fig. 5C,D). Moreover, we hypothesized that the
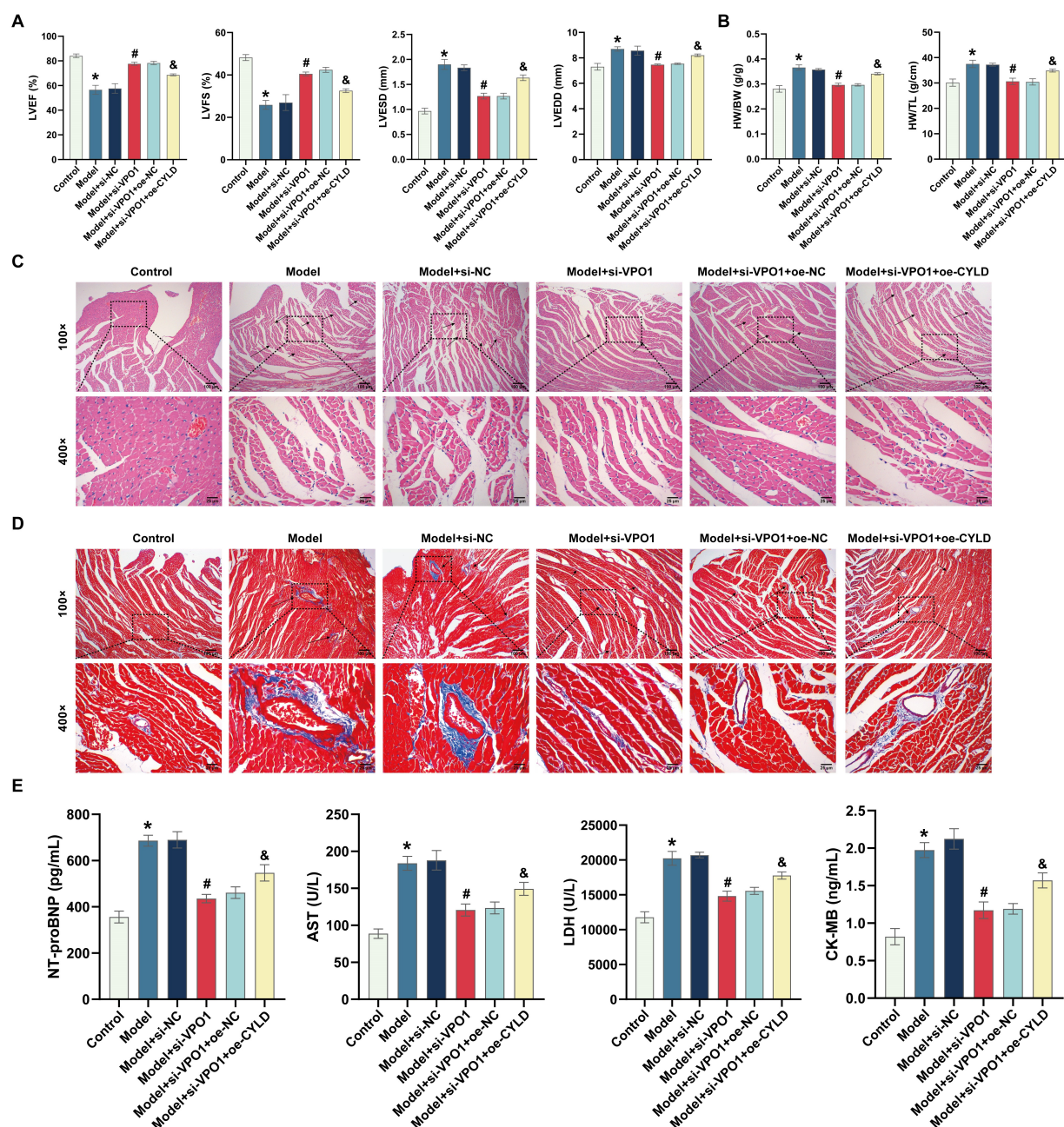
Fig. 5. VPO1 downregulation improves ADR-induced CHF in rats via the CYLD/RIPK1 axis. (A) Cardiac function was assessed by echocardiography measuring LVEF, LVFS, LVESD, and LVEDD. (B) Ratios of HW/BW and HW/TL were calculated. (C) Myocardial damage was evaluated using HE staining. The arrows represent the areas of myocardial injury. 400× scale bar = 25 μm, 100× scale bar = 100 μm. (D) Myocardial fibrosis was assessed by Masson staining. The arrows represent the areas of myocardial fibrosis. 400× scale bar = 25 μm, 100× scale bar = 100 μm. (E) Serum levels of NT-proBNP, AST, LDH, and CK-MB were measured. $^{*}p < 0.05$ vs. Control. $^{\#}p < 0.05$ vs. Model + si-NC. $^{\&}p < 0.05$ vs. Model + si-VPO1 + oe-NC. n = 5. HW/BW, weight/body weight; HW/TL, heart weight/tibia length; LVEF, left ventricular ejection fraction; LVFS, left ventricular fractional shortening; LVESD, left ventricular end-systolic diameter; LVEDD, left ventricular end-diastolic diameter; NT-proBNP, N-terminal pro b-type natriuretic peptide; AST, Aspartate aminotransferase; CK-MB, creatine kinase-myocardial band.

levels of cardiac injury-related factors NT-proBNP, AST, LDH, and CK-MB in serum. CHF raised the levels of NT-proBNP, AST, LDH, and CK-MB, suggesting that cardiac injury was increased, and our results showed that VPO1 downregulation reduced the NT-proBNP, AST, LDH, and CK-MB levels. Overexpression of *CYLD* reversed the mit-
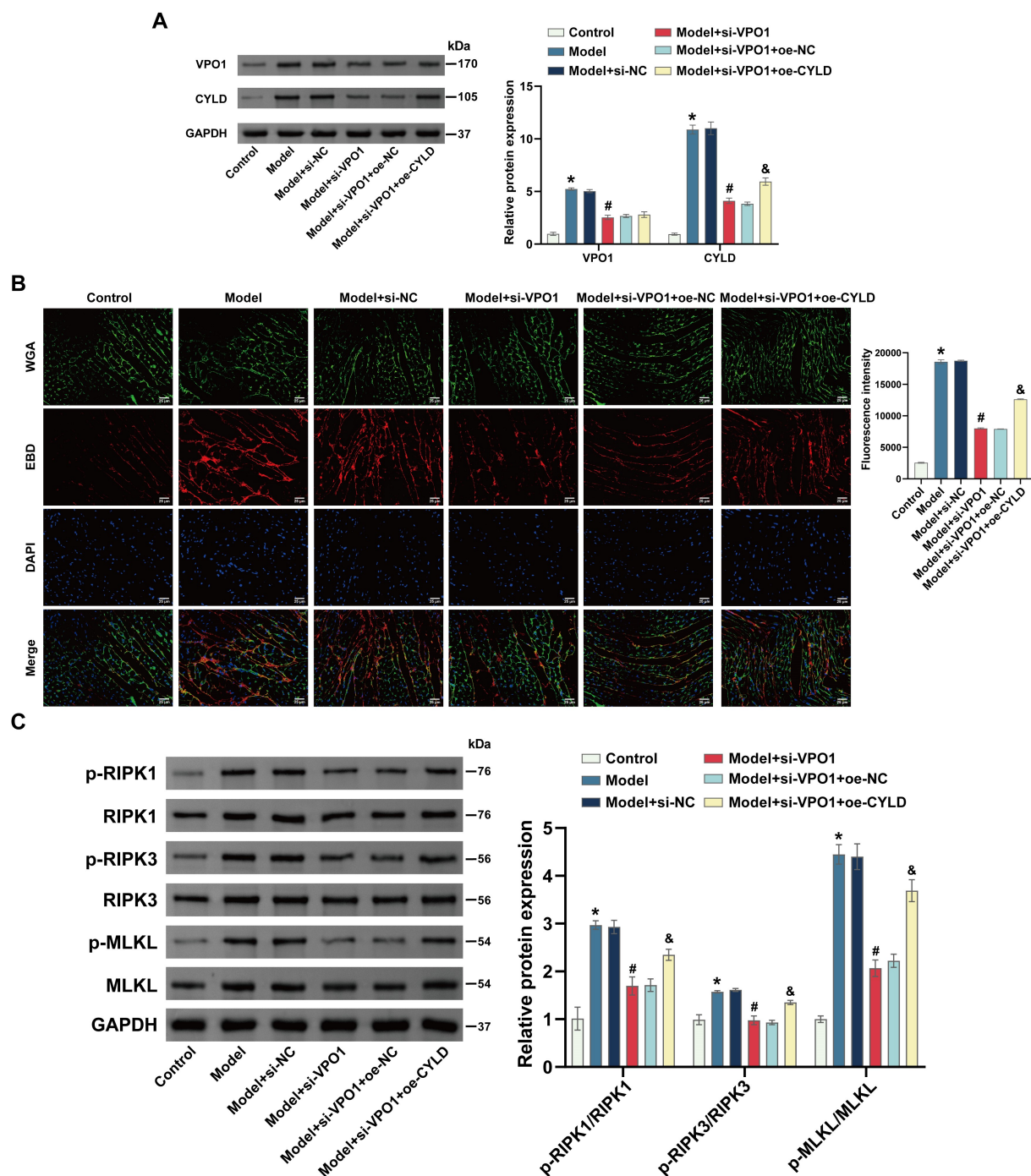
Fig. 6. VPO1 downregulation improves ADR-induced programmed necrosis of rat myocardial cells via the CYLD/RIPK1 axis.
(A) Levels of VPO1 and CYLD were examined by WB. (B) Myocardial tissue necrosis was evaluated by immunofluorescence (IF). Scale bar = 25 μm. (C) Levels of p-RIPK1/RIPK1, p-RIPK3/RIPK3, and p-MLKL/MLKL were measured by WB. $^*p < 0.05$ vs. Control. $^#p < 0.05$ vs. Model + si-NC. $^&p<0.05$ vs. Model + si-VPO1 + oe-NC. n = 5.

igating effects of VPO1 downregulation on cardiac injury (Fig. 5E). The above results postulated that downregulation of VPO1 could improve ADR-induced CHF in rats via the CYLD/RIPK1 axis.

3.6 VPO1 Downregulation Improves ADR-Induced Programmed Necrosis of Rat Myocardial Cells via the CYLD/RIPK1 Axis

We further validated whether VPO1 downregulation could improve ADR-induced programmed necrosis of rat

myocardial cells through the CYLD/RIPK1 axis. *VPO1* knockdown reversed the ADR-induced elevation of both VPO1 and CYLD levels. In contrast to the Model + si-VPO1 + oe-NC group, overexpression of *CYLD* enhanced CYLD levels without significantly altering VPO1 levels (Fig. 6A), indicating that changes in CYLD expression did not affect VPO1 levels. To assess myocardial cell necrosis, we applied WGA to localize myocardial cells and EBD to label damaged cells [37,38]. IF analysis implicated that VPO1 downregulation lowered myocardial cell necrosis in rats, whereas *CYLD* overexpression reversed this effect (Fig. 6B). Additionally, *CYLD* overexpression negated the reductions in phosphorylation of RIPK1, RIPK3, and MLKL caused by *VPO1* knockdown (Fig. 6C). These findings confirmed that VPO1 downregulation improved ADR-induced programmed necrosis of rat myocardial cells via the CYLD/RIPK1 axis.

4. Discussion

The treatment of CHF remains a prominent area of research [39]. This study highlighted the role of VPO1 in CHF, demonstrating that VPO1 activated the RIPK1/RIPK3/MLKL signaling pathway by upregulating CYLD, thereby promoting programmed necrosis of cardiomyocytes in rats. Our investigation into VPO1's role in CHF is a novel contribution to the field.

VPO1 is primarily expressed in endothelial and smooth muscle cells of the cardiovascular system [21]. It plays a critical role in myocardial ischemia-reperfusion injury, endothelial cell apoptosis, and smooth muscle cell proliferation through oxidative stress [40–42]. Furthermore, VPO1 influences conditions such as atherosclerosis and myocardial fibrosis [23,43]. In this study, we observed increased VPO1 expression in ADR-induced CHF rats, aligning with its known involvement in cardiovascular diseases. Additionally, VPO1 was found in cardiomyocytes, fibroblasts, and endothelial cells in the heart, suggesting a potential link between VPO1 expression and cardiac function. The activity and level of LDH are commonly used to evaluate tissue damage or cell lysis [44]. The RIPK1/RIPK3/MLKL pathway is a crucial signaling mechanism for programmed cell necrosis [45]. In our cellular experiments, ADR-induced programmed necrosis in H9c2 cells was mitigated by *VPO1* knockdown, which improved cell viability, reduced LDH levels, and decreased cell necrosis. Additional experiments suggested that VPO1 promotes CHF progression, possibly through its interaction with the deubiquitinase CYLD. This interaction contributed to the ubiquitination and degradation of RIPK1, thereby modulating cardiomyocyte necrosis via the RIPK1/RIPK3/MLKL signaling pathway.

The deubiquitinases CYLD, A20, OTUD1, OTUD7b, and OTULIN are known to regulate RIPK1 [30–34]. Our study found that only *VPO1* knockdown specifically reduced CYLD levels, with CYLD overexpression not affecting VPO1 levels, suggesting that CYLD functions downstream of VPO1. Previous research indicates that CYLD regulates the nuclear factor-κB (NF-κB) signaling pathway through its deubiquitinating activity [46], and NF-κB signaling is known to exacerbate CHF [47]. Thus, CYLD's role in CHF could be significant. In squamous cell carcinoma of the skin, CYLD deletion has been associated with increased tumor cell proliferation and metastasis [48]. CYLD also inhibits apoptosis by promoting the deubiquitination and degradation of apoptosis-related proteins [49]. Our data revealed that *CYLD* overexpression reversed the effects of *VPO1* knockdown in H9c2 cells, indicating that VPO1 regulated programmed necrosis through CYLD modulation.

Our present study further validated the effects of *VPO1* knockdown on ADR-induced CHF in rats. Evaluation of cardiac structure and function was performed using LVEF, LVFS, LVESD, and LVEDD [50,51]. Myocardial fibrosis, which contributes to myocardial stiffness and impairs heart function and contraction, was assessed [52]. Additionally, myocardial injury was estimated through serum levels of NT-proBNP, BNP, AST, and CK-MB [53]. Research has demonstrated that VPO1 mitigates oxidative damage in the heart [41], and VPO1 signaling may also regulate mitochondrial fragmentation and senescence in cardiomyocytes [54]. In our study, *CYLD* overexpression reversed the benefits of *VPO1* knockdown, including the reduction in heart failure, myocardial hypertrophy, myocardial injury, myocardial fibrosis, and myocardial cell necrosis observed in rats. These findings suggested that VPO1 may influence RIPK1 ubiquitination through CYLD, thereby modulating cardiac structure and function via the RIPK1/RIPK3/MLKL pathway, and playing a protective role in CHF development. Moreover, the interaction between VPO1 and CYLD appeared to have a significant regulatory impact on CHF pathogenesis. Beyond its role in ubiquitination, we hypothesized that this interaction might also influence NF-κB-related signaling pathways, inflammation, and cellular senescence.

Our findings indicated that VPO1 could be an effective target for CHF treatment. By modulating the expression or interaction of VPO1 and CYLD, it may intervene in the RIPK1/RIPK3/MLKL signaling pathway, thereby reducing programmed necrosis of cardiomyocytes and improving cardiac structure and function. However, several technical challenges remain, such as the time and cost associated with translating these findings into clinical applications, and the need for individualized treatment strategies and interventions targeting VPO1 and CYLD.

Despite these promising results, the study had some limitations. While we confirmed the interaction between VPO1 and CYLD, further research is needed to elucidate the detailed molecular mechanisms underlying this interaction and its involvement in additional signaling pathways. Furthermore, as the current study relies on a rat model,

clinical research is essential to determine whether drug-mediated inhibition of VPO1 can effectively improve heart failure in human patients.

5. Conclusions

In summary, this study demonstrated that VPO1 promoted programmed necrosis of cardiomyocytes in rats with CHF by upregulating CYLD and activating the RIPK1/RIPK3/MLKL signaling pathway. These findings offered new insights into the pathophysiological mechanisms underlying CHF and highlight VPO1 as a potential target for future heart failure treatments. Future research will focus on exploring additional molecular signaling pathways involving VPO1 and CYLD and examining the role of VPO1 within the clinical context of CHF.

Abbreviations

CHF, Chronic heart failure; VPO1, Vascular peroxidase 1; CYLD, cylindromatosis; LDH; lactate dehydrogenase; ACE, angiotensin-converting enzyme; DMEM, Dulbecco's modified Eagle's; si-NC, small interfering RNA-negative control; oe-NC, overexpressed negative control; CHX, cycloheximide; ECL, enhanced chemiluminescence; CCK-8, Cell counting kit-8; IHC, Immunohistochemistry; WB, Western Blot; RT-qPCR, Reverse transcription-quantitative polymerase chain reaction; IF, Immunofluorescence; WGA, Wheat Germ Agglutinin; LVEF, Left ventricular ejection fraction; LVFS, left ventricular fractional shortening; HW/TL, heart weight/tibia length; HW/BW, heart weight/body weight; SD, standard deviation.

Availability of Data and Materials

The datasets used and analyzed during the current study are available from the corresponding author on reasonable request.

Author Contributions

YZ and LF designed the experimental framework. LF provided the administrative support. ZS and ZM collected the data. YZ, DH and CL visualized the data. YZ, ZS and LF analyzed the data. YZ, ZS and ZM wrote the draft of the manuscript. All authors reviewed the manuscript. All authors read and approved the final manuscript. All authors have participated sufficiently in the work and agreed to be accountable for all aspects of the work.

Ethics Approval and Consent to Participate

All experimental procedures and animal handling were performed with the approval of the Animal Care and Use Committee of the Affiliated Changsha Hospital of Xiangya School of Medicine, Central South University (No. 2021-69), in accordance with the National Institutes of Health Guide for the Care and Use of Laboratory Animals, and studies involving laboratory animals follows the ARRIVE guidelines.

Acknowledgment

Not applicable.

Funding

Conflict of Interest

The authors declare no conflict of interest.

Supplementary Material

Supplementary material associated with this article can be found, in the online version, at https://doi.org/10.31083/j.fbl2912425.

References

[1] Mascolo A, di Mauro G, Cappetta D, De Angelis A, Torella D, Urbanek K, et al. Current and future therapeutic perspective in chronic heart failure. Pharmacological Research. 2022; 175: 106035. https://doi.org/10.1016/j.phrs.2021.106035.

[2] Angélico-Gonçalves A, Leite AR, Neves JS, Saraiva F, Brochado L, Oliveira AC, et al. Changes in health-related quality of life and treatment effects in chronic heart failure: a meta-analysis. International Journal of Cardiology. 2023; 386: 65–73. https://doi.org/10.1016/j.ijcard.2023.05.032.

[3] Koshy AO, Gallivan ER, McGinlay M, Straw S, Drozd M, Toms AG, et al. Prioritizing symptom management in the treatment of chronic heart failure. ESC Heart Failure. 2020; 7: 2193–2207. https://doi.org/10.1002/ehf2.12875.

[4] Wintrich J, Kindermann I, Böhm M. Update on heart failure. Herz. 2020; 45:158–169. https://doi.org/10.1007/s00059-018-4715-1. (In German)

[5] Steichert M, Cawello W, Bajcetic M, Breur JMPJ, Dalinghaus M, Male C, et al. Influence of Age, Heart Failure and ACE Inhibitor Treatment on Plasma Renin Activity in Children: Insights from a Systematic Review and the European LENA Project. Frontiers in bioscience (Landmark edition). 2023; 28: 335. https://doi.org/10.31083/j.fbl2812335.

[6] Vaduganathan M, Claggett BL, Jhund PS, Cunningham JW, Pedro Ferreira J, Zannad F, et al. Estimating lifetime benefits of comprehensive disease-modifying pharmacological therapies in patients with heart failure with reduced ejection fraction: a comparative analysis of three randomised controlled trials. Lancet (London, England). 2020; 396: 121–128. https://doi.org/10.1016/S0140-6736(20)30748-0.

[7] Mtisi TF, Frishman WH. Beta Adrenergic Blocker Use in Patients with Chronic Obstructive Pulmonary Disease and Concurrent Chronic Heart Failure with a Low Ejection Fraction. Cardiology in Review. 2020; 28: 20–25. https://doi.org/10.1097/CRD.0000000000000284.

[8] Huang D, Hua W, Fang Q, Yan J, Su Y, Liu B, et al. Biventricular pacemaker and defibrillator implantation in patients with chronic heart failure in China. ESC Heart Failure. 2021; 8: 546–554. https://doi.org/10.1002/ehf2.13114.

[9] Tani H, Sadahiro T, Yamada Y, Isomi M, Yamakawa H, Fujita R, *et al*. Direct Reprogramming Improves Cardiac Function and Reverses Fibrosis in Chronic Myocardial Infarction. Circulation. 2023; 147: 223–238. https://doi.org/10.1161/CIRCULATIONAHA.121.058655.

[10] Del Re DP, Amgalan D, Linkermann A, Liu Q, Kitsis RN. Fundamental Mechanisms of Regulated Cell Death and Implications for Heart Disease. Physiological Reviews. 2019; 99: 1765–1817. https://doi.org/10.1152/physrev.00022.2018.

[11] Liang QQ, Shi ZJ, Yuan T, Chen SY, Li YP, Zhang HR, *et al*. Celastrol inhibits necroptosis by attenuating the RIPK1/RIPK3/MLKL pathway and confers protection against acute pancreatitis in mice. International Immunopharmacology. 2023; 117: 109974. https://doi.org/10.1016/j.intimp.2023.109974.

[12] Lin P, Lin C, He R, Chen H, Teng Z, Yao H, *et al*. TRAF6 regulates the abundance of RIPK1 and inhibits the RIPK1/RIPK3/MLKL necroptosis signaling pathway and affects the progression of colorectal cancer. Cell Death & Disease. 2023; 14: 6. https://doi.org/10.1038/s41419-022-05524-y.

[13] Shi FL, Yuan LS, Wong TS, Li Q, Li YP, Xu R, *et al*. Dimethyl fumarate inhibits necroptosis and alleviates systemic inflammatory response syndrome by blocking the RIPK1-RIPK3-MLKL axis. Pharmacological Research. 2023; 189: 106697. https://doi.org/10.1016/j.phrs.2023.106697.

[14] Ahn D, Prince A. Participation of Necroptosis in the Host Response to Acute Bacterial Pneumonia. Journal of Innate Immunity. 2017; 9: 262–270. https://doi.org/10.1159/000455100.

[15] Marín-Rubio JL, Raote I, Inns J, Dobson-Stone C, Rajan N. CYLD in health and disease. Disease Models & Mechanisms. 2023; 16: dmm050093. https://doi.org/10.1242/dmm.050093.

[16] Yang C, Ran Q, Zhou Y, Liu S, Zhao C, Yu X, *et al*. Doxorubicin sensitizes cancer cells to Smac mimetic via synergistic activation of the CYLD/RIPK1/FADD/caspase-8-dependent apoptosis. Apoptosis: an International Journal on Programmed Cell Death. 2020; 25: 441–455. https://doi.org/10.1007/s10495-020-01604-6.

[17] Legarda D, Justus SJ, Ang RL, Rikhi N, Li W, Moran TM, *et al*. CYLD Proteolysis Protects Macrophages from TNF-Mediated Auto-necroptosis Induced by LPS and Licensed by Type I IFN. Cell Reports. 2016; 15: 2449–2461. https://doi.org/10.1016/j.celrep.2016.05.032.

[18] Kuroe T, Watanabe R, Morisue R, Miyazaki S, Kojima M, Murata SC, *et al*. Dirty necrosis in renal cell carcinoma is associated with NETosis and systemic inflammation. Cancer Medicine. 2023; 12: 4557–4567. https://doi.org/10.1002/cam4.5249.

[19] Wang Z, Li L, Liao S, Huang R, Jiang Y, Fei J, et al. Canthaxanthin Attenuates the Vascular Aging or Endothelial Cell Senescence by Inhibiting Inflammation and Oxidative Stress in Mice. Frontiers in bioscience (Landmark edition). 2023; 28: 367. https://doi.org/10.31083/j.fbl2812367.

[20] Yang W, Liu Z, Xu Q, Peng H, Chen L, Huang X, *et al*. Involvement of vascular peroxidase 1 in angiotensin II-induced hypertrophy of H9c2 cells. Journal of the American Society of Hypertension: JASH. 2017; 11: 519–529.e1. https://doi.org/10.1016/j.jash.2016.08.002.

[21] Liu Z, Liu Y, Xu Q, Peng H, Tang Y, Yang T, *et al*. Critical role of vascular peroxidase 1 in regulating endothelial nitric oxide synthase. Redox Biology. 2017; 12: 226–232. https://doi.org/10.1016/j.redox.2017.02.022.

[22] Li T, Liu B, Luo XJ, Peng J. VPO1/HOCl/ERK pathway mediates the right ventricular remodeling in rats with hypoxic pulmonary hypertension. Archives of Biochemistry and Biophysics. 2022; 723: 109267. https://doi.org/10.1016/j.abb.2022.109267.

[23] Liu Z, Xu Q, Yang Q, Cao J, Wu C, Peng H, *et al*. Vascular

[24] peroxidase 1 is a novel regulator of cardiac fibrosis after myocardial infarction. Redox Biology. 2019; 22: 101151. https://doi.org/10.1016/j.redox.2019.101151.

Zhu HJ, Han ZY, He SF, Jin SY, Xu SJ, Fang XD, *et al*. Specific MicroRNAs comparisons in hypoxia and morphine preconditioning against hypoxia-reoxgenation injury with and without heart failure. Life Sciences. 2017; 170: 82–92. https://doi.org/10.1016/j.lfs.2016.11.028.

[25] Zhong N, Nong X, Diao J, Yang G. piRNA-6426 increases DNMT3B-mediated SOAT1 methylation and improves heart failure. Aging. 2022; 14: 2678–2694. https://doi.org/10.18632/aging.203965.

[26] Zhang QL, Yang JJ, Zhang HS. Carvedilol (CAR) combined with carnosic acid (CAA) attenuates doxorubicin-induced cardiotoxicity by suppressing excessive oxidative stress, inflammation, apoptosis and autophagy. Biomedicine & Pharmacotherapy = Biomedecine & Pharmacotherapie. 2019; 109: 71–83. https://doi.org/10.1016/j.biopha.2018.07.037.

[27] Guo X, Zhu R, Luo A, Zhou H, Ding F, Yang H, *et al*. EIF3H promotes aggressiveness of esophageal squamous cell carcinoma by modulating Snail stability. Journal of Experimental & Clinical Cancer Research: CR. 2020; 39: 175. https://doi.org/10.1186/s13046-020-01678-9.

[28] Sharma P, Gentile C. Cardiac Spheroids as in vitro Bioengineered Heart Tissues to Study Human Heart Pathophysiology. Journal of Visualized Experiments: JoVE. 2021; 10.3791/61962. https://doi.org/10.3791/61962.

[29] Cummings BS, Schnellmann RG. Measurement of Cell Death in Mammalian Cells. Current Protocols. 2021; 1: e210. https://doi.org/10.1002/cpz1.210.

[30] Xu X, Kalac M, Markson M, Chan M, Brody JD, Bhagat G, *et al*. Reversal of CYLD phosphorylation as a novel therapeutic approach for adult T-cell leukemia/lymphoma (ATLL). Cell Death & Disease. 2020; 11: 94. https://doi.org/10.1038/s41419-020-2294-6.

[31] Iorga A, Donovan K, Shojaie L, Johnson H, Kwok J, Suda J, *et al*. Interaction of RIPK1 and A20 modulates MAPK signaling in murine acetaminophen toxicity. The Journal of Biological Chemistry. 2021; 296: 100300. https://doi.org/10.1016/j.jbc.2021.100300.

[32] Wu B, Qiang L, Zhang Y, Fu Y, Zhao M, Lei Z, *et al*. The deubiquitinase OTUD1 inhibits colonic inflammation by suppressing RIPK1-mediated NF-κB signaling. Cellular & Molecular Immunology. 2022; 19: 276–289. https://doi.org/10.1038/s41423-021-00810-9.

[33] Harit K, Bhattacharjee R, Matuschewski K, Becker J, Kalinke U, Schlüter D, *et al*. The deubiquitinating enzyme OTUD7b protects dendritic cells from TNF-induced apoptosis by stabilizing the E3 ligase TRAF2. Cell Death & Disease. 2023; 14: 480. https://doi.org/10.1038/s41419-023-06014-5.

[34] Schünke H, Göbel U, Dikic I, Pasparakis M. OTULIN inhibits RIPK1-mediated keratinocyte necroptosis to prevent skin inflammation in mice. Nature Communications. 2021; 12: 5912. https://doi.org/10.1038/s41467-021-25945-1.

[35] Li T, Jin J, Pu F, Bai Y, Chen Y, Li Y, *et al*. Cardioprotective effects of curcumin against myocardial I/R injury: A systematic review and meta-analysis of preclinical and clinical studies. Frontiers in Pharmacology. 2023; 14: 1111459. https://doi.org/10.3389/fphar.2023.1111459.

[36] Yue P, Zhang Y, Liu L, Zhou K, Xia S, Peng M, *et al*. *Yap1* modulates cardiomyocyte hypertrophy via impaired mitochondrial biogenesis in response to chronic mechanical stress overload. Theranostics. 2022; 12: 7009–7031. https://doi.org/10.7150/thno.74563.

[37] Wang K, Li FH, Zhou LY, Zhao XM, Gao XQ, Liu CY, *et al*. HNEAP Regulates Necroptosis of Cardiomyocytes by Sup-

pressing the m^5 C Methylation of Atf7 mRNA. Advanced Science (Weinheim, Baden-Wurttemberg, Germany). 2023; 10: e2304329. https://doi.org/10.1002/advs.202304329.

[38] Xiao P, Wang C, Li J, Su H, Yang L, Wu P, *et al*. COP9 Signalosome Suppresses RIPK1-RIPK3-Mediated Cardiomyocyte Necroptosis in Mice. Circulation. Heart Failure. 2020; 13: e006996. https://doi.org/10.1161/CIRCHEARTFAILURE.120.006996.

[39] Trochu JN. Chronic heart failure with reduced EF: A decade of major pharmacological innovations. Presse Medicale (Paris, France: 1983). 2024; 53: 104219. https://doi.org/10.1016/j.lpm.2023.104219.

[40] Cui S, Lv X, Li W, Li Z, Liu H, Gao Y, *et al*. Folic acid modulates VPO1 DNA methylation levels and alleviates oxidative stress-induced apoptosis in vivo and in vitro. Redox Biology. 2018; 19: 81–91. https://doi.org/10.1016/j.redox.2018.08.005.

[41] Zhang YS, Lu LQ, Jiang YQ, Li NS, Luo XJ, Peng JW, *et al*. Allopurinol attenuates oxidative injury in rat hearts suffered ischemia/reperfusion via suppressing the xanthine oxidase/vascular peroxidase 1 pathway. European Journal of Pharmacology. 2021; 908: 174368. https://doi.org/10.1016/j.ejphar.2021.174368.

[42] You B, Liu Y, Chen J, Huang X, Peng H, Liu Z, *et al*. Vascular peroxidase 1 mediates hypoxia-induced pulmonary artery smooth muscle cell proliferation, apoptosis resistance and migration. Cardiovascular Research. 2018; 114: 188–199. https://doi.org/10.1093/cvr/cvx234.

[43] Yang Y, Shi R, Cao Z, Zhang G, Cheng G. VPO1 mediates oxidation of LDL and formation of foam cells. Oncotarget. 2016; 7: 35500–35511. https://doi.org/10.18632/oncotarget.9193.

[44] Farhana A, Lappin SL. Biochemistry, Lactate Dehydrogenase. StatPearls: Treasure Island (FL). 2024.

[45] Xu X, Fan X, Wu X, Xia R, Liang J, Gao F, *et al*. Luteolin ameliorates necroptosis in Glucocorticoid-induced osteonecrosis of the femoral head via RIPK1/RIPK3/MLKL pathway based on network pharmacology analysis. Biochemical and Biophysical Research Communications. 2023; 661: 108–118. https://doi.org/10.1016/j.bbrc.2023.04.023.

[46] Minderman M, Lantermans HC, Grüneberg LJ, Cillessen SAGM, Bende RJ, van Noesel CJM, *et al*. MALT1-dependent cleavage of CYLD promotes NF-κB signaling and growth of aggressive B-cell receptor-dependent lymphomas. Blood Cancer Journal. 2023; 13: 37. https://doi.org/10.1038/s41408-023-00809-7.

[47] Wu YX, Xu RY, Jiang L, Chen XY, Xiao XJ. MicroRNA-30a-5p Promotes Chronic Heart Failure in Rats by Targeting Sirtuin-1 to Activate the Nuclear Factor-κB/NOD-Like Receptor 3 Signaling Pathway. Cardiovascular Drugs and Therapy. 2023; 37: 1065–1076. https://doi.org/10.1007/s10557-021-07304-w.

[48] Cui Z, Kang H, Grandis JR, Johnson DE. CYLD Alterations in the Tumorigenesis and Progression of Human Papillomavirus-Associated Head and Neck Cancers. Molecular Cancer Research: MCR. 2021; 19: 14–24. https://doi.org/10.1158/1541-7786.MCR-20-0565.

[49] Zhang X, Zhao Y, Zhang X, Shen G, Li W, Wang Q. Deubiquitinase cylindromatosis (CYLD) regulates antibacterial immunity and apoptosis in Chinese mitten crab (Eriocheir sinensis). Fish & Shellfish Immunology. 2023; 132: 108454. https://doi.org/10.1016/j.fsi.2022.108454.

[50] Yan J, Li Z, Liang Y, Yang C, Ou W, Mo H, *et al*. Fucoxanthin alleviated myocardial ischemia and reperfusion injury through inhibition of ferroptosis *via* the NRF2 signaling pathway. Food & Function. 2023; 14: 10052–10068. https://doi.org/10.1039/d3fo02633g.

[51] Chen YC, Hsing SC, Chao YP, Cheng YW, Lin CS, Lin C, *et al*. Clinical Relevance of the LVEDD and LVESD Trajectories in HF Patients With LVEF < 35. Frontiers in Medicine. 2022; 9: 846361. https://doi.org/10.3389/fmed.2022.846361.

[52] López B, Ravassa S, Moreno MU, José GS, Beaumont J, González A, *et al*. Diffuse myocardial fibrosis: mechanisms, diagnosis and therapeutic approaches. Nature Reviews. Cardiology. 2021; 18: 479–498. https://doi.org/10.1038/s41569-020-00504-1.

[53] Sun S, Dawuti A, Gong D, Wang R, Yuan T, Wang S, *et al*. Puerarin-V Improve Mitochondrial Respiration and Cardiac Function in a Rat Model of Diabetic Cardiomyopathy via Inhibiting Pyroptosis Pathway through P2X7 Receptors. International Journal of Molecular Sciences. 2022; 23: 13015. https://doi.org/10.3390/ijms232113015.

[54] Zheng H, Liang X, Liu B, Huang X, Shen Y, Lin F, *et al*. Exosomal miR-9-5p derived from iPSC-MSCs ameliorates doxorubicin-induced cardiomyopathy by inhibiting cardiomyocyte senescence. Journal of Nanobiotechnology. 2024; 22: 195. https://doi.org/10.1186/s12951-024-02421-8.